RSC Advances

PAPER

View Article Online
View Journal | View Issue

Cite this: *RSC Adv.*, 2025, **15**, 10484

Comprehensive assessment of 3-benzyloxyflavones as β-glucosidase inhibitors: *in vitro*, *in vivo*, kinetic, SAR and computational studies†

Nafeesa Naeem and Ehsan Ullah Mughal *

Received 4th December 2024
Accepted 15th March 2025

DOI: 10.1039/d4ra08558b

rsc.li/rsc-advances

In this study, a series of 3-benzyloxyflavone derivatives (**1–10**) was designed and, for the first time, evaluated for both *in vitro* and *in vivo* inhibitory activity against the β-glucosidase enzyme. The enzyme inhibitory potential of these derivatives was further assessed in an antihyperglycemic context using *in vivo* mechanism-based assays on *p*-nitrophenyl-β-D-glucopyranoside (PGLT) induced diabetic models. Additionally, structure–activity relationship (SAR) was employed to identify structural features crucial for activity. Molecular docking analyses revealed that both the potent compounds and co-crystallized ligands shared similar binding orientations within the active sites of β-glucosidase (PDB IDs: 3AJ7; 66K1). Molecular dynamics (MD) simulations validated the stability of the inhibitor–enzyme complexes under physiological conditions, while density functional theory (DFT) calculations helped elucidate electronic properties critical for activity. Drug-likeness analysis was also conducted to assess the pharmacokinetic potential of the derivatives. The results highlighted several derivatives with significant inhibitory activity, desirable pharmacokinetic profiles, and promising drug-like properties, making them potential candidates for therapeutic development. The target derivatives (**1–10**) demonstrated strong potential as lead compounds for developing new anti-diabetic agents with effective anti-hyperglycemic properties.

1. Introduction

β-Glucosidase is an essential enzyme involved in the hydrolysis of β-glycosidic bonds in β-D-glucosides, oligosaccharides, and other complex carbohydrates, leading to the release of glucose and other monosaccharides.[1] This enzyme plays a pivotal role in biological processes like cellulose degradation, where it aids in breaking down cellobiose into glucose, which is essential for energy production in microorganisms.[2] Additionally, β-glucosidase is crucial in the metabolism of glycosides in plants and mammals, contributing to defense mechanisms and lysosomal degradation, respectively.[3] The deficiency of β-glucosidase in humans is linked to lysosomal storage disorders such as Gaucher's disease, highlighting its clinical importance.[4]

In microorganisms, especially fungi, and bacteria, β-glucosidase is an important component of the cellulolytic enzyme system, facilitating the complete saccharification of cellulose by converting cellobiose into glucose.[5,6] In plants, the enzyme contributes to defense mechanisms, as it helps in the release of bioactive compounds from glycosides in response to external stress or pathogen attack.[7–9] In mammals, β-glucosidase plays a role in the lysosomal degradation of glycosphingolipids, with its deficiency leading to disorders such as Gaucher's disease.[4,10]

In industrial biotechnology, β-glucosidase has attained significant attention due to its role in biofuel production, particularly in the enzymatic breakdown of lignocellulosic biomass.[11] Its ability to enhance the saccharification process by hydrolyzing cellobiose into glucose has made it a key target in optimizing bioethanol production.[6,12] Additionally, β-glucosidase plays a critical role in the food and beverage industry, where it helps release flavor-enhancing compounds from glycosides in fruits and wines.[13,14]

Flavonoids, as naturally occurring polyphenolic structures, have drawn extensive interest in scientific research due to their wide-ranging biological activities, including antioxidant, anti-inflammatory, anticancer, and enzyme-inhibitory properties.[15–22] 3-*O*-Benzylflavonol, commonly known as 3-benzyloxyflavone (Fig. 1), represents a prominent subclass within the broader category of flavonoid compounds, characterized by the substitution of a benzyloxy group at the third position of the flavonol core. These are one of the pharmacologically active synthetic derivatives of flavonols.[23,24] The structural modification in 3-benzyloxyflavone not only enhances its hydrophobic nature but also confers unique molecular interactions that have been linked to increased biological efficacy.[25–27] This

Department of Chemistry, University of Gujrat, Gujrat-50700, Pakistan. E-mail: ehsan.ullah@uog.edu.pk

† Electronic supplementary information (ESI) available. See DOI: https://doi.org/10.1039/d4ra08558b

modification impacts its pharmacokinetic profile, remarkably improving cellular permeability and enzyme-binding affinity.[28,29] Recent research highlights the compound's enhanced interaction with hydrophobic enzyme active sites, particularly glycosidases like β-glucosidase, making it a promising candidate for enzyme inhibition.[30,31] The compound's structural flexibility and synthetic accessibility further support its potential as a lead molecule for designing analogs with optimized selectivity and biological efficacy.[32,33]

Research into β-glucosidase inhibition has gained importance, particularly in the context of discovering new therapeutic agents for managing diseases such as type-2 diabetes and Gaucher's disease.[34,35] Traditional inhibitors like acarbose have been effective in controlling glucose metabolism by inhibiting glucosidases, but the search for more potent and selective inhibitors continues.[36–38] Recent studies have shown that flavonoids, including flavones and their derivatives, exhibit significant inhibitory activity against β-glucosidase.[39,40] These compounds act by interacting with the active site of the enzyme, preventing the hydrolysis of glucosidic substrates.[41,42]

Among flavonoids, 3-benzyloxyflavones have emerged as promising candidates due to their unique structure–activity relationship (SAR) that enhances their binding affinity to β-glucosidase. Their ability to inhibit the enzyme has been attributed to the presence of the benzyloxy group, which enhances lipophilicity and facilitates interactions with hydrophobic regions of the enzyme's active site.[43,44] These flavones are also being studied for their ability to modulate other biological targets, expanding their therapeutic potential beyond enzyme inhibition.[45,46]

Additionally, to the best of our knowledge, for the first time, this motif has been evaluated against β-glucosidase. Recent advancements in computational docking studies, alongside *in vitro*, and *in vivo* enzyme assays, have provided valuable insights into the molecular interactions between 3-benzyloxyflavones and β-glucosidase. These studies have not only confirmed their inhibitory potential but also provided a framework for optimizing their structure for enhanced activity and selectivity. This growing body of evidence suggests that 3-benzyloxyflavones could serve as promising leads for developing novel glucosidase inhibitors with applications in both therapeutic and industrial applications.

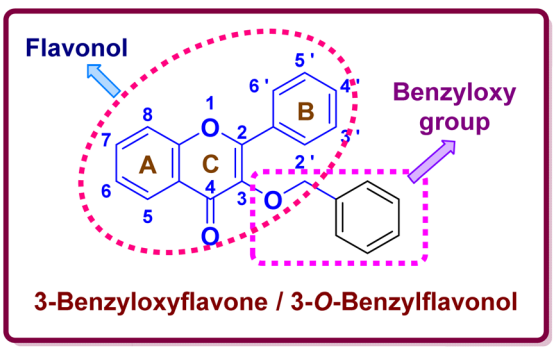

Fig. 1 Representative structure of 3-*O*-benzylflavonol or 3-benzyloxyflavone.

2. Experimental section

2.1. General procedure for the synthesis of 3-benzyloxyflavones (1–10)

The 3-benzyloxyflavones (**1–10**) were synthesized according to the procedure outlined in our previously published literature.[23]

2.2. Enzyme inhibitory assay

2.2.1. *In vitro* β-glucosidase inhibitory assay. Compounds (**1–10**) were evaluated for their inhibitory activity against β-glucosidase, according to the procedure given in the literature.[47,48] Test samples were prepared by combining 20 μL of β-glucosidase (0.5 U mL^{-1}), 120 μL of 0.1 M phosphate buffer at pH 6.9, and 10 μL of compounds (**1–10**) at varying concentrations. The reaction mixtures were incubated in 96-well plates at 37 °C for 15 minutes. The enzymatic reaction was initiated by adding 20 μL of a 5 mM solution of *p*-nitrophenyl-β-D-glucopyranoside prepared in 0.1 M phosphate buffer (pH 6.9), followed by an additional incubation at 37 °C for 15 minutes. The reaction was speed up by adding 80 μL of 0.2 M sodium carbonate. Absorbance was then measured at 405 nm using a microplate reader. A sample-free reaction system served as the positive control, while a blank without β-glucosidase was included to correct for background absorbance. The inhibitory activity was quantified as a percentage relative to a control sample that did not contain any inhibitors (eqn (1)).

$$\% \text{ inhibition} = \frac{\text{absorbance of control} - \text{absorbance of sample}}{\text{absorbance of control}} \times 100 \quad (1)$$

2.2.2. *In vivo* β-glucosidase inhibitory assay. The *in vivo* β-glucosidase inhibitory assay was conducted following the methodology described in our previously published studies,[7,48–50] with the detailed experimental procedure provided in the ESI file.†

2.3. Kinetic assay

A kinetic study was carried out to evaluate the inhibition mechanism of the most potent compounds **8** and **10** against β-glucosidase using earlier methodology.[48,51] For compound **8**, 20 μL of enzyme solution (1 U mL^{-1}) was incubated at 37 °C with varying concentrations of the inhibitor (0, 55, 75, and 95 μM). The reaction was initiated by adding *p*-nitrophenyl-β-D-glucopyranoside (PGLT) (1–4 mM) as the substrate, and absorbance changes were monitored at 405 nm for 20 minutes. Lineweaver–Burk plots were used to identify the mode of inhibition, and the Michaelis–Menten constant (K_m) and inhibition constant (K_i) were calculated. Additionally, compound **10** was examined under the same conditions at inhibitor concentrations of 0, 30, 50, and 75 μM, with absorbance recorded over 20 minutes using a Gen5 PowerWave XS2 spectrophotometer (BioTek, USA).

2.4. Computational studies

2.4.1. Molecular docking analysis. The molecular docking assay was carried out following the methodology described in

our previous literature,[52–54] with the detailed procedure provided in the ESI file.† The anti-diabetic medication acarbose serves as a reference compound when the compounds are molecularly docked. Table 6 lists the ligands found in proteins along with their resolution, year, and organism. Table S1 in the ESI file† provides detailed data on the MolDock score, the number of hydrogen bonds, the compound names and categories, bond types, interaction distances, and the amino acid residues involved in hydrogen bonding.

2.4.2. MD simulation. To assess the stability of the protein–ligand complex, a 100 ns molecular dynamics (MD) simulation was performed. The system was solvated in a periodic cubic box with a 10 Å buffer zone filled with TIP3P water molecules.[55] Sodium (Na^+) and chloride (Cl^-) ions were added to neutralize the system. Energy minimization was carried out using the steepest descent algorithm for 5000 steps to eliminate steric clashes following system neutralization. Post-minimization, the system underwent equilibration in two phases: 50 000 steps under the NVT ensemble and 100 000 steps under the NPT ensemble at 310 K.[56] The Berendsen thermostat and Parrinello–Rahman barostat were employed to maintain a constant temperature (310 K) and pressure (1 atm). Relaxation of the system was achieved with time constants (τ_P) of 2.0 ps for pressure and (τ_T) of 0.1 ps for temperature. The LINCS algorithm was used to constrain hydrogen bond lengths to their equilibrium positions,[57] while the Verlet algorithm calculated non-bonded interactions.[58] Long-range electrostatic interactions were computed using the Particle Mesh Ewald (PME) method.[59] Periodic boundary conditions were applied in all three dimensions (x, y, z), and a production MD run was executed. Trajectories were saved every 10 ps and analyzed using the R BIO3D package and GROMACS commands[60] The CHARMM36 force field and GROMACS simulation software were utilized to perform the MD simulation.[61]

2.4.3. DFT study. All hypothetical calculations on the reference medication and lead docking compounds were completed with the help of the designed Gauss View 6.0.16 and Gaussian16 software as well as the density functional theory framework. Becke's three-parameter hybrid exchange–correlation functional (B3LYP) and the 6-311G basis set were used to study the frontier molecular orbitals, optimized geometry parameters, and molecular electrostatic potential (MEP). The DFT parameters display the dipole moment, electronegativity, energy gap, chemical potential, and hardness and softness.[62] The 6-311G basis set with the B3LYP functional is selected because it offers a favorable trade-off between accuracy and computing efficiency, especially for organic compounds. This combination is appropriate for predicting structural, electrical, and reactive properties since it accurately captures electron correlation and polarization effects.

2.4.4. Drug-likeness assay. The drug-likeness of the compounds (**1–10**) was evaluated based on their physicochemical and pharmacokinetic properties, following a systematic approach.[47] Compounds were chosen according to their structural features and preliminary biological activity. Key properties, including molecular weight, log P, and the counts of hydrogen bond donors and acceptors, were calculated using cheminformatics software *i.e.*, ChemAxon. The compounds were then screened against Lipinski's rule of five to ensure they met the thresholds for molecular weight (<500 Da), log P (<5), hydrogen bond donors (≤5), and acceptors (≤10). Furthermore, compounds were assessed for synthetic accessibility and a bioavailability score to predict their oral bioavailability.

3. Results and discussion

3.1. Chemistry

The synthesis of 3-*O*-benzylated flavonols/3-benzyloxyflavones (**1–10**) (Scheme 1), was achieved using the established Algar–Flynn–Oyamada (AFO) reaction. The spectroscopic data for all synthesized 3-benzyloxyflavones (**1–10**) can be found in our previous publication.[23]

3.2. β-Glucosidase inhibitory activity

The 3-benzyloxyflavone derivatives (**1–10**) were evaluated for their *in vitro* inhibitory potential against the β-glucosidase enzyme, with IC_{50} values measured to assess their activity (Table 1). Among the derivatives, compound **8** demonstrated the most potent inhibitory effect with an IC_{50} = 0.17 μM, indicating a strong affinity for β-glucosidase. This was followed by compound **3**, which also showed significant activity with an IC_{50} = 0.22 μM. In contrast, compound **1** displayed the lowest inhibitory activity among the series, with an IC_{50} = 1.02 μM, though still showing effectiveness.

Furthermore, other derivatives exhibited moderate inhibitory activity, with IC_{50} values ranging from 0.25 μM (compound **10**) to 0.51 μM (compound **2**). All target compounds showed greater potency compared to the standard reference, acarbose (IC_{50} = 34.09 μM). These results indicate that the benzyloxyflavone framework is effective in generating potent β-glucosidase inhibitors, with certain structural features likely enhancing binding affinity and enzyme interaction. The SAR for these derivatives suggests that specific substitutions within the benzyloxyflavone core may contribute to variations in potency. These findings indicate that derivatives like **3**, **5**, **6**, **7**, **8**, and **10** have potential as lead candidates for developing new β-glucosidase inhibitors for antihyperglycemic therapy.

3.3. *In vivo* study

3.3.1. Acute toxicity. The compounds **3**, **5**, **6**, **7**, **8** and **10** exhibited no mortality in animals administered a maximum oral dose of 2000 mg per kg (b.w.). The animals were observed daily for a period of two weeks, during which no signs of toxicity, such as diarrhea, convulsions, lethargy, sedation, salivation, or tremors, were noted. Based on these toxicity findings, an effective dose of 200 mg kg^{-1} ($1/10^{th}$ of the maximum dose) was established. Subsequently, lower doses of 5 and 7.5 mg kg^{-1} were chosen for behavioral studies following an initial pharmacological evaluation conducted in our laboratory.

3.3.2. Estimation of blood glucose level. The blood glucose levels of benzyloxyflavone derivative-treated groups were monitored over 28 days, with significant reductions observed in glucose concentrations across the tested doses (Table 2). The

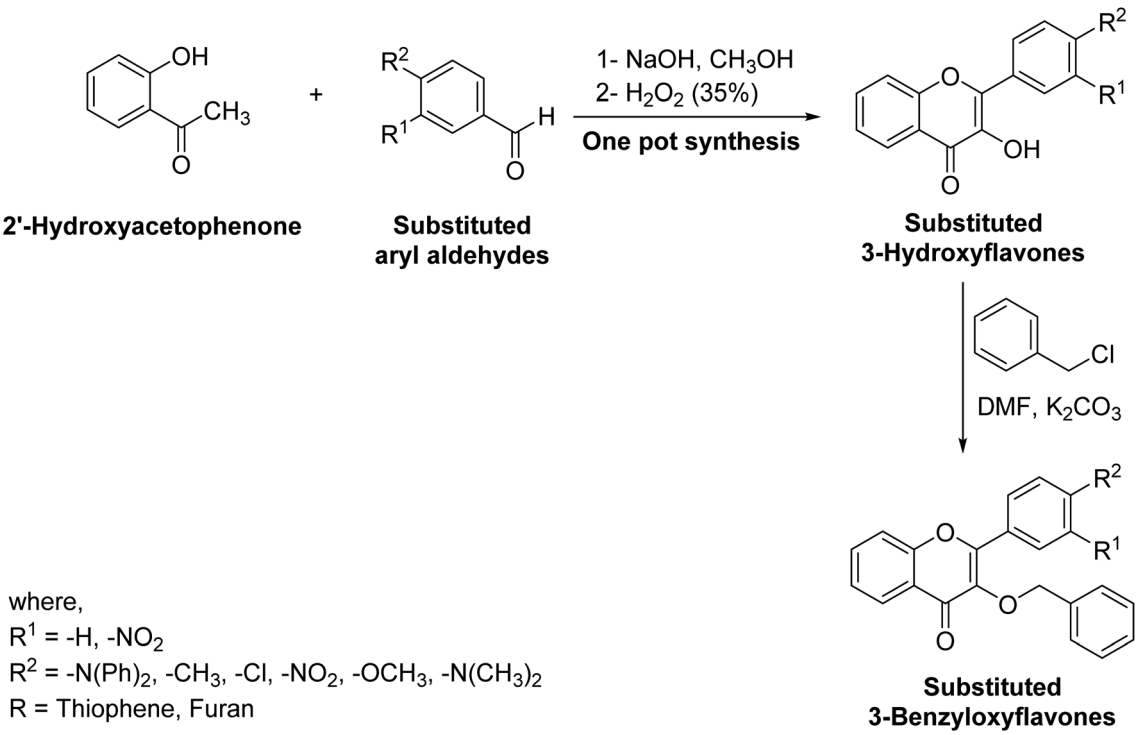

Scheme 1 Synthesis of 3-benzyloxyflavone derivatives (**1–10**).

diabetic control group displayed consistently elevated glucose levels, beginning at 397.61 ± 5.04 mg dL^{-1} on day 1 and remaining above 396 mg dL^{-1} throughout the study, confirming sustained hyperglycemia without intervention.

Among the benzyloxyflavone derivatives, compound **8** exhibited notable antidiabetic effects. At 5 mg kg^{-1}, glucose levels decreased from 401.69 ± 5.31 mg dL^{-1} on day 1 to 126.13 ± 4.91 mg dL^{-1} on day 28, representing the most substantial reduction across the derivatives tested. At 7.5 mg kg^{-1}, compound **8** showed a similar trend, reducing glucose levels from 395.48 ± 4.24 mg dL^{-1} on day 1 to 139.28 ± 5.61 mg dL^{-1} by day 28. Other derivatives, such as compounds **3**, **6**, **7**, and **5**, also demonstrated dose-dependent decreases in blood glucose, although to a lesser degree than compound **8**.

Compound **3**, administered at 5 mg kg^{-1}, decreased glucose levels from 398.51 ± 4.91 mg dL^{-1} initially to 142.84 ± 4.90 mg dL^{-1} by day 28. At 7.5 mg kg^{-1}, it further reduced levels to 149.62 ± 3.89 mg dL^{-1}. Compound **6** also showed progressive reductions, with glucose levels at 153.19 ± 4.73 mg dL^{-1} at 5 mg kg^{-1} and 148.25 ± 3.98 mg dL^{-1} at 7.5 mg kg^{-1} by the end of the study period. Compounds **7**, **5**, and **10** demonstrated a similar gradual decline, with compound **5** at 5 mg kg^{-1} reducing glucose from 398.40 ± 4.68 mg dL^{-1} to 135.81 ± 4.51 mg dL^{-1} by day 28, marking it as one of the more effective derivatives in the lower dose range.

For comparison, the positive control, *p*-nitrophenyl-β-D-glucopyranoside (PGLT), at 10 mg kg^{-1}, significantly lowered glucose levels from 402.22 ± 4.97 mg dL^{-1} on day 1 to near-normal levels of 102.27 ± 4.31 mg dL^{-1} on day 28. This outcome underscores the potency of PGLT as a standard antidiabetic agent.

Overall, these results indicate that benzyloxyflavone derivatives possess significant antihyperglycemic potential, with compound **8** emerging as the most promising candidate due to its substantial impact on glucose reduction. The lower dose (5 mg kg^{-1}) demonstrated effective glucose control across several derivatives, suggesting that further exploration of benzyloxyflavone structures may yield potent candidates for antidiabetic therapy.

3.3.3. Effects on body weights. The changes in body weight for control and experimental rats treated with the compounds and PGLT are shown in Table 3. Diabetic rats induced with PGLT experienced a significant weight loss ($^{**}P < 0.01$, $n = 8$) compared to normal rats. The diabetic control group showed the highest weight loss at 28.81%, while the treated groups generally exhibited a lower weight loss percentage, with the PGLT group showing only 2.48%, indicating a reduction in weight loss potentially due to the intervention. The normal control group maintained a consistent body weight throughout the study, indicating stable health. In contrast, the diabetic control group exhibited a significant weight reduction from day 1 to day 28, reflecting the typical weight loss observed in diabetic conditions.

Treatment with the test compounds at both 5 mg kg^{-1} and 7.5 mg kg^{-1} doses led to a moderation in weight loss compared to the diabetic control. For example, compound **3** at 7.5 mg kg^{-1} prevented significant weight loss, maintaining a relatively stable weight profile, similar to the control. Other compounds, including **5**, **6**, and **8** at both doses, also demonstrated

Table 1 β-Glucosidase inhibitory activity of 3-benzyloxyflavones (**1–10**)

Compound no.	Chemical structure	β-Glucosidase $IC_{50} \pm SEM^a$ (μM)
1	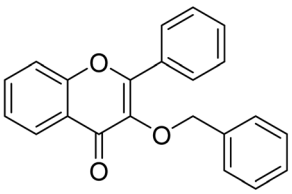 **3-(Benzyloxy)-2-phenyl-4*H*-chromen-4-one**	1.02 ± 0.02
2	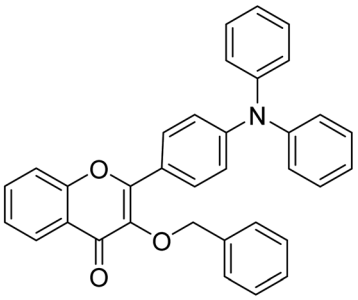 **3-(Benzyloxy)-2-(4-(diphenylamino)phenyl)-4*H*-chromen-4-one**	0.51 ± 0.26
3	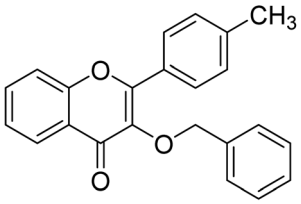 **3-(Benzyloxy)-2-(*p*-tolyl)-4*H*-chromen-4-one**	0.28 ± 0.05
4	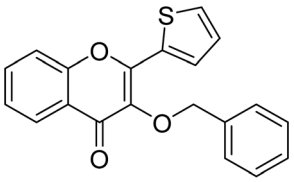 **3-(Benzyloxy)-2-(thiophen-2-yl)-4*H*-chromen-4-one**	0.42 ± 0.08
5	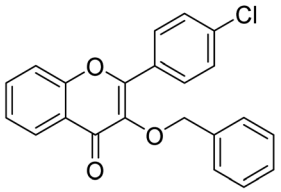 **3-(Benzyloxy)-2-(4-chlorophenyl)-4*H*-chromen-4-one**	0.36 ± 0.19
6	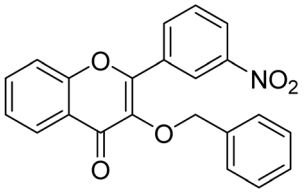 **3-(Benzyloxy)-2-(3-nitrophenyl)-4*H*-chromen-4-one**	0.30 ± 0.11

Table 1 (*Contd.*)

Compound no.	Chemical structure	β-Glucosidase $IC_{50} \pm SEM^a$ (μM)
7	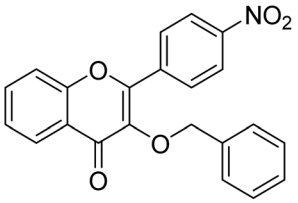 3-(Benzyloxy)-2-(4-nitrophenyl)-4*H*-chromen-4-one	0.37 ± 0.13
8	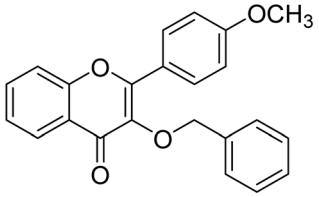 3-(Benzyloxy)-2-(4-methoxyphenyl)-4*H*-chromen-4-one	0.17 ± 0.05
9	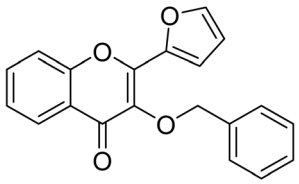 3-(Benzyloxy)-2-(furan-2-yl)-4*H*-chromen-4-one	0.39 ± 0.14
10	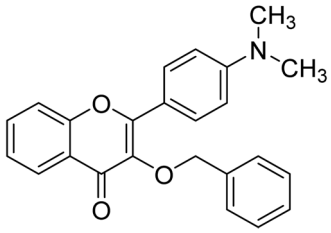 3-(Benzyloxy)-2-(4-(dimethylamino)phenyl)-4*H*-chromen-4-one	0.25 ± 0.12
Acarbose (standard)	—	34.09 ± 1.07

[a] IC_{50} values (mean ± standard error of the mean).

protective effects on body weight, although to varying extents. The PGLT (10 mg) treated group exhibited weight maintenance comparable to that of the normal control, validating its protective efficacy. However, treatment with the selected compounds at doses of 5 and 7.5 mg per kg b.w. effectively reversed the PGLT-induced weight loss. Remarkably, these findings suggest that several benzyloxyflavone derivatives at appropriate dosages can positively influence body weight maintenance in diabetic models, potentially reflecting broader antidiabetic properties.

3.3.4. Antihyperlipidemic effects. Lipid profile analysis was conducted for each test animal to evaluate potential side effects associated with the administered compounds, as presented in Table 4. In the diabetic group, significant increases in total cholesterol (CH), triglycerides (TGs), and LDL levels were observed ($^*P < 0.05$, $^{**}P < 0.01$, $^{***}P < 0.001$, $n = 8$) compared to the normal control group. Furthermore, diabetic rats exhibited a notable reduction in HDL levels ($^*P < 0.05$, $n = 8$). Treatment with the test compounds at doses of 5 mg kg^{-1} and 7.5 mg kg^{-1} over 28 days resulted in a significant decrease in TGs, total cholesterol, and LDL levels ($^*P < 0.05$, $^{**}P < 0.01$, $^{***}P < 0.001$, $n = 8$), with outcomes comparable to those achieved by standard therapeutic agents.

Table 2 Effect on blood glucose in PGLT-induced diabetes[a]

Blood glucose level in mg per dL per day						
Groups		1st	7th	14th	21st	28th
Normal control		107.81 ± 5.12	110.32 ± 4.81	106.70 ± 4.91	108.51 ± 4.59	103.21 ± 4.41
Diabetic control		397.61 ± 5.04$^{!!!}$	412.37 ± 4.88$^{!!!}$	409.57 ± 4.98$^{!!!}$	401.45 ± 5.03$^{!!!}$	396.21 ± 4.79$^{!!!}$
3	5 mg	398.51 ± 4.91	332.97 ± 4.89	218.68 ± 4.90*	172.59 ± 4.80**	142.84 ± 4.90**
	7.5 mg	400.63 ± 5.12	329.73 ± 3.96	278.39 ± 4.98*	189.47 ± 5.00**	149.62 ± 3.89**
5	5 mg	398.40 ± 4.68	334.91 ± 4.81**	209.93 ± 4.77**	175.86 ± 4.79**	135.81 ± 4.51***
	7.5 mg	440.70 ± 4.97	340.47 ± 4.25**	235.85 ± 4.97**	190.56 ± 5.32**	139.86 ± 4.64***
6	5 mg	393.37 ± 4.71	341.56 ± 4.71*	235.71 ± 4.68**	185.67 ± 4.91**	153.19 ± 4.73**
	7.5 mg	400.52 ± 4.89	335.72 ± 4.48*	240.93 ± 4.90**	182.58 ± 4.63**	148.25 ± 3.98**
7	5 mg	401.06 ± 5.02	339.11 ± 4.90*	243.12 ± 4.79*	188.70 ± 4.65*	165.39 ± 4.88*
	7.5 mg	407.17 ± 4.99	328.42 ± 4.54*	287.53 ± 5.38*	198.87 ± 4.80*	161.16 ± 4.41*
8	5 mg	401.69 ± 5.31	306.17 ± 4.58**	194.85 ± 4.97***	148.70 ± 4.83***	126.13 ± 4.91***
	7.5 mg	395.48 ± 4.24	310.19 ± 5.10**	192.77 ± 4.46***	158.92 ± 4.14***	139.28 ± 5.61***
10	5 mg	407.17 ± 4.12	331.39 ± 4.73*	208.09 ± 4.88*	169.60 ± 4.63**	137.70 ± 4.89**
	7.5 mg	467.53 ± 5.48	325.44 ± 4.89*	210.16 ± 4.56*	164.57 ± 4.42**	140.81 ± 4.90**
p-Nitrophenyl-β-D-glucopyranoside (PGLT)	10 mg	402.22 ± 4.97	229.56 ± 4.80***	154.06 ± 4.59***	119.70 ± 4.87***	102.27 ± 4.31***

[a] All values are presented as mean ± SEM, with $n = 8$. Statistical significance was evaluated using one-way ANOVA followed by Dunnett's *post hoc* multiple comparison test. Significance levels were denoted as follows: $^{!!!}P < 0.001$ for diabetic control *versus* normal control; $^{*}P < 0.05$, $^{**}P < 0.01$, and $^{***}P < 0.001$ for comparisons between diabetic control and both test samples and *p*-nitrophenyl-β-D-glucopyranoside-treated groups.

Table 3 Effect of the target compounds on the body weights of rats[a]

Groups/dose mg kg^{-1}		1st day	7th day	14th day	21st day	28th day
Normal control		20.34 ± 2.18	21.71 ± 2.01	21.41 ± 1.89	20.61 ± 2.18	20.98 ± 1.94
Diabetic control		21.31 ± 1.52	20.56 ± 1.90	18.41 ± 1.48	17.30 ± 1.70	15.17 ± 1.39
3	5 mg	22.07 ± 1.81	22.11 ± 1.67	20.50 ± 1.69	20.11 ± 1.81	19.41 ± 1.61
	7.5 mg	22.51 ± 1.73	21.98 ± 1.74	20.87 ± 1.66	20.24 ± 1.78	19.75 ± 1.68
5	5 mg	20.70 ± 1.73	20.66 ± 1.90	19.48 ± 1.53	19.34 ± 1.71	18.96 ± 1.81
	7.5 mg	21.04 ± 1.79	20.83 ± 1.69	19.92 ± 1.60	19.58 ± 1.74	19.03 ± 1.77
6	5 mg	19.97 ± 1.81	18.91 ± 1.58	18.65 ± 1.79	18.03 ± 1.48	18.16 ± 1.77
	7.5 mg	20.28 ± 1.80	19.32 ± 1.54	18.79 ± 1.64	18.27 ± 1.56	18.34 ± 1.65
7	5 mg	21.41 ± 1.73	21.16 ± 1.81	20.64 ± 1.87	19.80 ± 1.70	17.91 ± 1.80
	7.5 mg	21.92 ± 1.76	21.37 ± 1.68	20.82 ± 1.75	19.93 ± 1.77	18.21 ± 1.75
8	5 mg	22.61 ± 1.98	21.12 ± 1.91	20.77 ± 1.88	20.69 ± 1.69	19.66 ± 1.72
	7.5 mg	22.88 ± 1.91	21.36 ± 1.76	21.03 ± 1.71	20.81 ± 1.74	20.13 ± 1.63
10	5 mg	19.84 ± 1.70	19.67 ± 1.66	19.34 ± 1.48	18.90 ± 1.60	18.75 ± 1.58
	7.5 mg	20.11 ± 1.72	19.85 ± 1.69	19.56 ± 1.51	19.12 ± 1.54	18.89 ± 1.60
PGLT	10 mg	20.16 ± 1.71	19.88 ± 1.81	20.01 ± 1.61	19.70 ± 1.69	19.66 ± 1.51

[a] All values are presented as means ± SEM, with $n = 8$. Statistical analysis was conducted using one-way ANOVA followed by Dunnett's *post hoc* test. Significant differences are indicated as follows: $^{!!!}P < 0.001$ for comparisons between diabetic and normal control groups, and $^{*}P < 0.05$, $^{**}P < 0.01$, $^{***}P < 0.001$ for comparisons between diabetic control and test groups or PGLT groups.

Triglycerides (TG): compounds **8** and **10** at both 5 mg kg^{-1} and 7.5 mg kg^{-1} showed substantial reductions in TG levels, approaching those of the standard PGLT-treated group. Remarkably, compound **5** at 7.5 mg kg^{-1} brought TG levels close to baseline values, demonstrating a remarkable lipid-lowering effect.

Total cholesterol (CH): treatment with compounds **8** and **10**, especially at the higher dose, resulted in significant reductions in total cholesterol. Compound **8** at 7.5 mg kg^{-1} showed a reduction close to that of the PGLT standard group, highlighting its potency in cholesterol management.

Low-density lipoprotein (LDL): most compounds effectively lowered LDL levels, with compounds **8** and **10** at 7.5 mg kg^{-1} producing the most pronounced effects. These results emphasize their ability to reduce atherogenic lipids, thus contributing to cardiovascular protection.

High-density lipoprotein (HDL): increased HDL levels were observed in animals treated with the derivatives, with compound **8** at 7.5 mg kg^{-1} showing the highest increase. Elevated HDL levels are beneficial, as they play a crucial role in reverse cholesterol transport.

Henceforth, these findings suggest that benzyloxyflavone derivatives, particularly compounds **8** and **10**, hold promising lead candidates for antihyperlipidemic treatment. Their lipid-regulating effects are comparable to standard treatments, and further investigations into their mechanisms could elucidate their potential therapeutic roles.

Table 4 Antihyperlipidemic effects on PGLT-induced diabetes[a]

Groups/dose mg kg^{-1}		TG (mg dL^{-1})	Total CH (mg dL^{-1})	LDL (mg dL^{-1})	HDL (mg dL^{-1})
Normal control		91.72 ± 3.72	102.44 ± 4.87	85.61 ± 2.02	57.91 ± 2.03
Diabetic control		176.80 ± 3.13$^{!!!}$	197.81 ± 5.03$^{!!!}$	189.70 ± 3.81$^{!!!}$	26.37 ± 1.80$^{!!!}$
3	5 mg	129.55 ± 3.76**	149.11 ± 4.80*	128.77 ± 3.41**	42.81 ± 1.90**
	7.5 mg	120.30 ± 3.59**	138.30 ± 4.72*	117.44 ± 3.29**	44.10 ± 1.84**
5	5 mg	136.30 ± 3.61**	145.33 ± 4.79**	124.79 ± 3.91**	45.34 ± 2.14*
	7.5 mg	130.00 ± 3.58**	140.20 ± 4.76**	118.44 ± 3.85**	46.10 ± 2.11*
6	5 mg	147.12 ± 4.03*	152.30 ± 4.80*	127.64 ± 3.39**	43.66 ± 1.98*
	7.5 mg	142.40 ± 4.01*	148.50 ± 4.77*	122.21 ± 3.31**	45.00 ± 1.94*
7	5 mg	145.34 ± 4.40*	160.04 ± 4.91*	140.39 ± 4.14**	39.90 ± 1.92**
	7.5 mg	138.20 ± 4.35*	153.80 ± 4.85*	135.02 ± 4.09**	41.02 ± 1.89**
8	5 mg	113.09 ± 4.41***	125.17 ± 4.92***	102.49 ± 3.19***	51.11 ± 2.01***
	7.5 mg	108.01 ± 4.28***	119.80 ± 4.89***	97.90 ± 3.10***	52.70 ± 2.08***
10	5 mg	130.09 ± 4.29**	135.56 ± 4.70**	113.60 ± 3.40***	46.89 ± 1.97*
	7.5 mg	125.20 ± 4.24**	130.21 ± 4.66**	110.08 ± 3.31***	48.02 ± 1.99*
PGLT	10 mg	96.36 ± 4.51***	104.73 ± 4.83***	87.58 ± 2.96***	55.72 ± 2.01***

[a] All values are presented as mean ± SEM, with $n = 8$ per group. Statistical significance was determined using one-way ANOVA followed by Dunnett's *post hoc* test. Significance levels are indicated as follows: $^{!!!}P < 0.001$ for diabetic control *versus* normal control, and $^{*}P < 0.05$, $^{**}P < 0.01$, $^{***}P < 0.001$ for diabetic control compared with test samples and the PGLT-treated group.

Table 5 Impact of compounds on serum biochemical parameters[a]

Groups/dose mg kg^{-1}		(SGOT) IU	(SGPT) IU	(ALP) IU
Normal control		21.15 ± 1.98	19.34 ± 1.67	169.83 ± 4.10
Diabetic control		47.53 ± 2.12$^{!!!}$	60.21 ± 2.44$^{!!!}$	288.67 ± 4.56$^{!!!}$
3	5 mg	26.96 ± 2.34**	38.21 ± 2.61**	198.77 ± 4.11*
	7.5 mg	24.55 ± 2.02**	33.78 ± 2.43*	192.11 ± 4.05**
5	5 mg	24.61 ± 2.06***	31.70 ± 2.11***	184.32 ± 4.09***
	7.5 mg	22.40 ± 2.10***	29.32 ± 2.21***	181.73 ± 4.08***
6	5 mg	31.41 ± 2.12**	44.56 ± 2.98*	210.70 ± 4.82**
	7.5 mg	28.69 ± 2.08**	40.91 ± 2.96*	205.56 ± 4.72**
7	5 mg	33.09 ± 2.31*	45.98 ± 3.04*	217.89 ± 4.90**
	7.5 mg	29.98 ± 2.15*	42.83 ± 3.00*	212.49 ± 4.80**
8	5 mg	32.44 ± 2.65**	38.69 ± 2.61**	197.65 ± 4.71*
	7.5 mg	28.62 ± 2.55**	33.40 ± 2.50**	193.43 ± 4.69*
10	5 mg	29.75 ± 2.40**	36.29 ± 2.40***	196.70 ± 4.11**
	7.5 mg	26.51 ± 2.31**	31.12 ± 2.35***	192.53 ± 4.03**
PGLT	10 mg	21.39 ± 1.79***	21.17 ± 1.88***	171.04 ± 3.91***

[a] Data are presented as mean ± SEM, with $n = 8$ per group. Statistical analysis was performed using one-way ANOVA followed by Dunnett's *post hoc* test. Significance levels are indicated as $^{!!!}P < 0.001$ for comparisons between the diabetic and normal control groups, and $^{*}P < 0.05$, $^{**}P < 0.01$, $^{***}P < 0.001$ for comparisons between the diabetic control and test groups, as well as the PGLT-treated group.

3.3.5. Effects on liver. The levels of hepatic marker enzymes, including serum glutamate oxaloacetate transaminase (SGOT), serum glutamate pyruvate transaminase (SGPT), and alkaline phosphatase (ALP) were elevated in the PGLT-induced diabetic group, as shown in Table 5 and Fig. 2A–C. Treatment with the tested compounds at doses of 5 and 7.5 mg kg^{-1} significantly reduced these serum biomarkers. Additionally, a notable decrease in creatinine levels was observed compared to the standard PGLT.

The liver enzyme profile of diabetic rats treated with benzyloxyflavone derivatives (compounds **3**, **5**, **6**, **7**, **8**, and **10**) showed a significant improvement in serum levels of SGOT, SGPT, and ALP compared to the untreated diabetic control group. Diabetic control rats displayed notably elevated levels of SGOT (47.53 ± 2.12 IU), SGPT (60.21 ± 2.44 IU), and ALP (288.67 ± 4.56 IU), indicating marked liver stress and potential hepatic dysfunction induced by the diabetic condition.

Among the tested compounds, compound **5** (7.5 mg) produced the most pronounced effects, reducing SGOT to 22.40 ± 2.10 IU, SGPT to 29.32 ± 2.21 IU, and ALP to 181.73 ± 4.08 IU, comparable to the levels observed in the PGLT-treated group, which is a standard for comparison. This suggests that compound **5** may have a protective effect on liver function, effectively lowering liver enzyme levels to near-normal values. Additionally, compounds **8** and **10** at 7.5 mg doses also exhibited substantial improvements, reducing SGOT, SGPT, and ALP levels significantly ($P < 0.05$ to $P < 0.001$) when compared to the diabetic control, demonstrating their potential for liver protection in diabetic states.

3.4. Kinetic study

Kinetic analysis of compound **8**, the most potent β-glucosidase inhibitor among the synthesized derivatives, revealed its competitive inhibition mode. This was determined through Lineweaver–Burk plotting, showing no change in V_{max} and an increase in K_m, with a K_i value of 90 μM (Fig. S1 in ESI file†). Additionally, the kinetic study of compound **10** also indicated competitive inhibition, as evidenced by the Lineweaver–Burk plot showing a constant V_{max} and an increased K_m. The K_i value for compound **10** was found to be 75 μM, based on the secondary replot derived from the Lineweaver–Burk plot (Fig. S2 in ESI file†).

3.5. Structure–activity relationship (SAR) based on the IC_{50} values against β-glucosidase

The SAR analysis of the synthesized 3-(benzyloxy)-2-aryl-4*H*-chromen-4-one derivatives reveals the influence of various

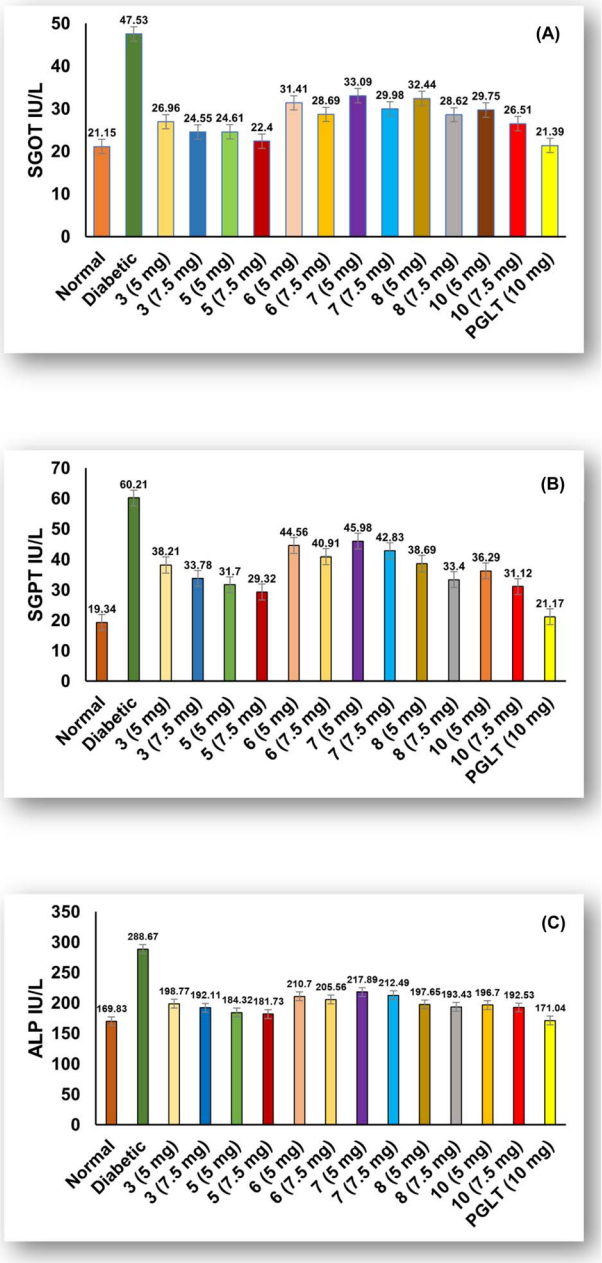

Fig. 2 Effects of compounds on serum profiles: (A) serum glutamic-oxaloacetic transaminase (SGOT), (B) serum glutamic pyruvic transaminase (SGPT), and (C) alkaline phosphatase (ALP). All values are presented as means ± SEM ($n = 8$). Statistical significance was assessed using one-way ANOVA followed by Dunnett's *post hoc* test. A comparison between the diabetic control group and the normal control group revealed significant differences ($^{!!!}P < 0.001$). Comparisons of the diabetic control group with test samples and PGLT-treated groups showed $^{*}P < 0.05$, $^{**}P < 0.01$, and $^{***}P < 0.001$.

substituents on β-glucosidase inhibitory activity (Fig. 3). Each compound's IC_{50} value indicates the effect of different aryl substitutions at the 2-position on the chromenone ring, highlighting both electron-donating and electron-withdrawing effects.

Compounds with electron-donating groups exhibit enhanced inhibitory activity. For example, compound **8**, containing a 4-methoxyphenyl group, shows the lowest IC_{50} value (0.17 μM), suggesting that electron-donating substituents contribute to increased activity by stabilizing interactions within the enzyme's active site. Similarly, compound **3**, with a *p*-tolyl group (an electron-donating methyl group on the phenyl ring), also demonstrates potent inhibition ($IC_{50} = 0.22$ μM), reinforcing the role of electron-donating effects in enzyme binding affinity.

On the other hand, the presence of electron-withdrawing groups generally results in moderate β-glucosidase inhibition. For instance, compound **7**, featuring a 4-nitrophenyl group, shows an IC_{50} of 0.37 μM, while compound **6**, with a 3-nitrophenyl group, yields an IC_{50} of 0.30 μM. The nitro group, known for its electron-withdrawing character, likely decreases the electron density on the aryl ring, leading to slightly lower binding efficacy in the enzyme's active site.

Furthermore, compound **5**, substituted with a 4-chlorophenyl group (electron-withdrawing chlorine), demonstrates moderate inhibition with an IC_{50} of 0.36 μM. Interestingly, heterocyclic substitutions like those in compounds **4** (thiophen-2-yl) and **9** (furan-2-yl) result in IC_{50} values of 0.42 μM and 0.39 μM, respectively. These heterocycles likely provide different steric and electronic properties, subtly influencing their inhibitory profiles.

Additionally, the diphenylamino substitution in compound **2** ($IC_{50} = 0.51$ μM) and the dimethylamino substitution in compound **10** ($IC_{50} = 0.25$ μM) highlight that more extensive π-conjugation and electron-donating nitrogen substituents can variably enhance binding, with smaller amino groups demonstrating stronger activity. Remarkably, all synthesized compounds show substantially higher activity compared to the standard, acarbose ($IC_{50} = 34.09$ μM), indicating a promising scaffold for β-glucosidase inhibition.

Henceforth, electron-donating substituents such as methoxy and methyl enhance β-glucosidase inhibition in the chromenone derivatives, while electron-withdrawing groups like nitro and chloro result in moderate activity, with slight differences arising from the distinct electronic and steric demands of each substituent. This SAR study provides insight into the optimized design of chromenone-based β-glucosidase inhibitors.

3.6. Computational studies

3.6.1. Molecular docking study. To confirm the potential of the synthesized compounds depending on their antidiabetic properties *in vitro* and *in vivo*, molecular docking was carried out as an *ex silico* investigation.[63] Using Molegro Virtual Docker (MVD), docking studies were performed to assess the binding affinities and interaction patterns of ten synthetic compounds against the antidiabetic protein targets 3AJ7 and 6KK1. The reference ligand was the well-known antidiabetic drug acarbose. **1**, **2**, **8**, **9**, and **10** showed good docking results among the compounds examined, suggesting they may be effective antidiabetic medicines (Tables 6 and S1 in the ESI file†).

3.6.2. Binding affinities. The degree of interaction between the compounds and the target proteins was confirmed by the

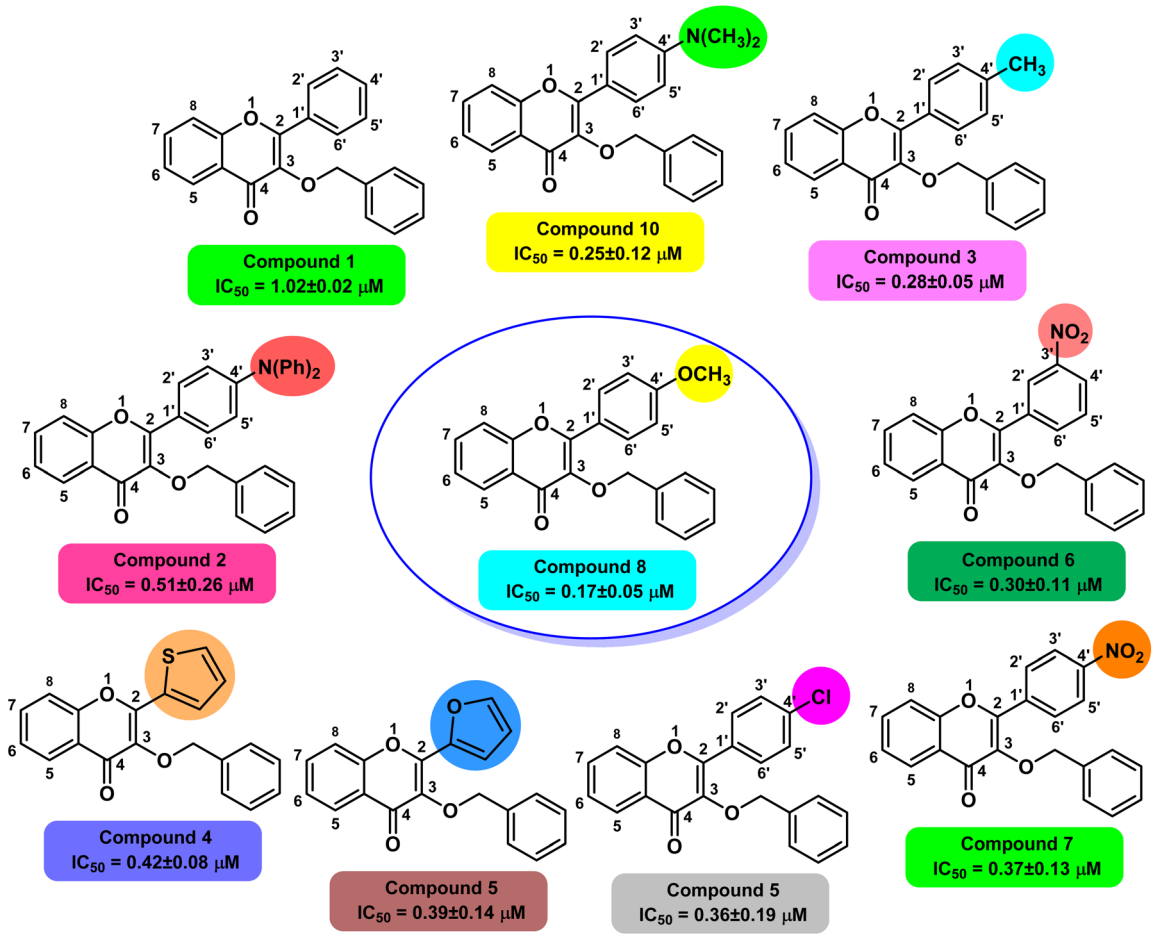

Fig. 3 SAR for β-glucosidase enzyme activity of 3-benzyloxyflavones (**1–10**).

Table 6 Proteins for anti-diabetic activity

Sr. no.	PDB ID	Resolution	Year	Ligand	Organism	Reference
1	3AJ7	1.30 Å	2010	Calcium ion	*Saccharomyces cerevisiae*	64
2	6KK1	2.80 Å	2019	*N*-{4-[(*R*)-(3,3-dimethylcyclobutyl)({6-[4-(trifluoromethyl)-1*H*-imidazol-1-yl] pyridin-3-yl}amino)methyl]benzene-1-carbonyl}-beta-alanine, $C_{26}H_{28}F_3N_5O_3$, MYZIDYJMNWEJMC-QHCPKHFHSA-N	*Homo sapiens*	65

Moldock scores. **1**'s Moldock score for 3AJ7 was −137.111, similar to that of acarbose (−146.731). **8** had a Moldock score of −117.927, indicating strong interactions, while **2** likewise demonstrated a favorable binding affinity with a value of −123.86. **10** outperformed acarbose (−82.2585) with a score of 102.675 against 6KK1, while **9** showed a good score of −94.5894, confirming their potential as powerful inhibitors. The compounds' biological activity and their binding affinities are in good agreement, indicating that they are effective antidiabetic medicines.[66]

3.6.3. Hydrogen bonding interactions. The stability of the protein–ligand complexes was primarily attributed to hydrogen bonding, with bond lengths ranging from 2.1 Å to 3.0 Å. Compounds **1** and **2** formed multiple hydrogen bonds with key residues in 3AJ7, including ARG315, GLN279, and ASP307. Compound **10** interacted with residues SER240, TYR158, and GLU411 in 6KK1, with bond lengths as short as 2.4 Å, while compound **8** established strong hydrogen bonds with ARG442, GLU277, and ASP352. These interactions confirm the compounds' ability to efficiently bind to the active sites of the target proteins, mimicking the bonding pattern of acarbose.[67]

3.6.4. Hydrophobic interactions. The binding stability of the selected compounds was further reinforced by hydrophobic interactions. Compound **9** formed strong hydrophobic contacts with residues PRO312 and LYS156, while compound **1** interacted with hydrophobic residues such as TYR158 and PHE314 in 3AJ7. Compound **10** demonstrated substantial binding within the hydrophobic pockets of 6KK1 through interactions

with VAL232, LEU313, and ARG315. These hydrophobic interactions contributed to the overall stability and enhanced binding affinity of the protein–ligand complexes.[68]

3.6.5. Comparison with acarbose. Acarbose exhibited strong binding affinities and interactions; however, the docking data for compounds **1**, **2**, **8**, **9**, and **10** demonstrated comparable or superior results (Table S1 in the ESI file†). For example, **10** showed a greater binding affinity towards 6KK1 with the highest Moldock score. The compounds' hydrogen bonding and hydrophobic interactions with key residues highlight their potential as effective inhibitors of the target proteins.[69]

Compounds **8** and **10**, identified as lead candidates in both *in vitro* and *in vivo* studies, display robust interactions with their respective target proteins, as shown in Fig. S3 and S4 in the ESI file,† outperforming the reference ligand, acarbose. The protein–ligand interaction diagrams illustrate that both compounds form hydrophobic contacts and stable hydrogen bonds with active site residues. The 2D interaction diagrams emphasize key hydrogen bond donors and acceptors that enhance binding efficiency, while the hydrophobic maps highlight the non-polar regions that contribute to ligand stability. Compound **8** demonstrates significant stability with 3AJ7 in Fig. S3 in the ESI file,† whereas compound **10** exhibits superior hydrophobic compatibility and binding energy with 6KK1 in Fig. S4 in the ESI file.† These results indicate that compounds **8** and **10** are potent inhibitors of both targets, with their strong hydrophobic interactions, high binding affinities, and substantial hydrogen bonding reinforcing their potential as effective antidiabetic agents.

3.6.6. Molecular dynamic simulation. The Root Mean Square Deviation (RMSD) of the Cα atoms of the protein was evaluated to assess the stability of the protein–ligand complex (compound **8**) (Fig. 4a). Initially, the RMSD of the protein increased steadily, reaching approximately 0.3 nm, followed by a slight deviation to 0.6 nm at 30 ns. Subsequently, the RMSD decreased to 0.13 nm. Between 30 and 50 ns, the RMSD fluctuated within a range of 0.13 to 0.2 nm, demonstrating stability after 50 ns, with an average RMSD value stabilizing around 0.17 to 0.2 nm.

To further investigate protein flexibility, the Root Mean Square Fluctuation (RMSF) was calculated and represented in a plot (Fig. 4b). High RMSF values correspond to flexible residues, while lower values indicate rigid regions. Significant fluctuations were observed in residues 75–95, 245–255, and 325–345, which correspond to loop regions. The remaining residues exhibited minimal fluctuations, suggesting that the protein retained its rigidity and did not undergo notable flexibility during the simulation.

The compactness of the protein structure was examined by calculating the radius of gyration (R_g) over the simulation period (Fig. 4c). Elevated R_g values indicate protein unfolding events. The R_g plot revealed that the protein maintained structural stability throughout the simulation, with values starting around ~2.05 nm and remaining consistent between ~2.06 and ~2.07 nm.

Additionally, hydrogen bonding between the protein and ligand was analyzed to evaluate the stability of the complex (Fig. 4d). A greater number of hydrogen bonds generally

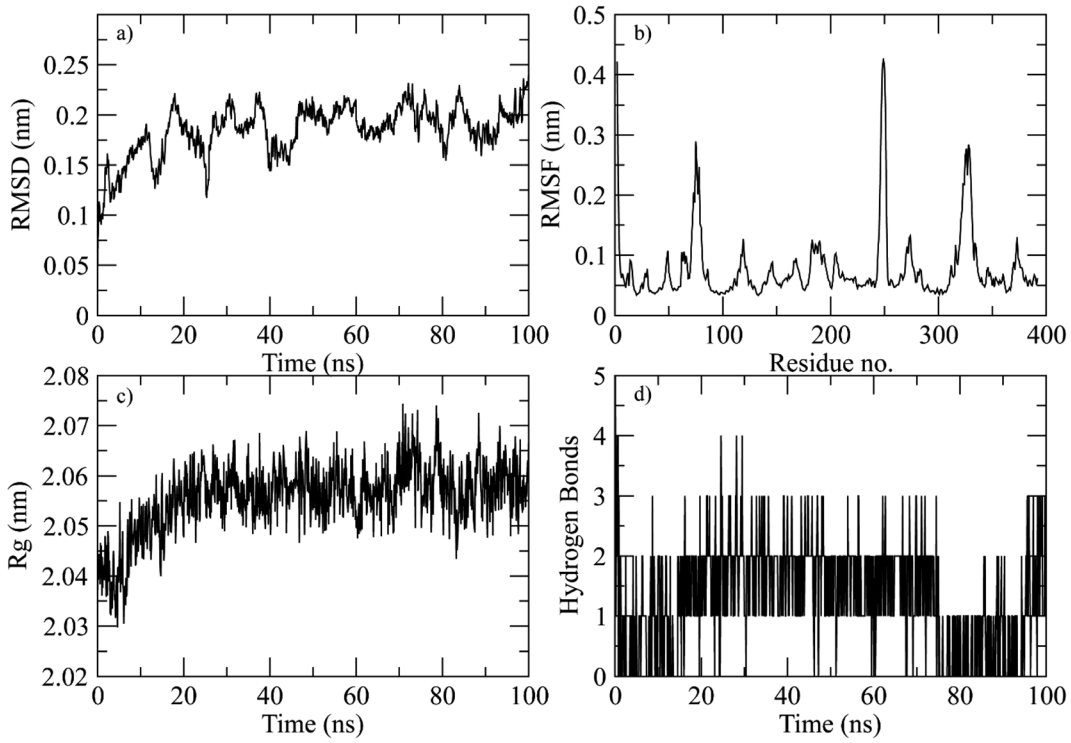

Fig. 4 MD trajectory analysis highlighting various stability parameters. (a) RMSD of the protein backbone atoms over the simulation. (b) RMSF plot depicting the flexibility of protein residues in the presence of the ligand. (c) R_g analysis reflects the structural compactness of the protein. (d) Hydrogen bonding profile showing the number of hydrogen bonds formed between the protein and the ligand during the simulation.

correlates with enhanced stability. At the beginning of the simulation, up to four hydrogen bonds were observed, which gradually decreased to three towards the end. The average number of hydrogen bonds throughout the simulation was 2.5, indicating strong binding and a stable protein–ligand complex.

3.6.7. DFT studies. The docking lead compounds **1**, **2**, **8**, **9**, and **10** were evaluated at the basic set of 6-311G/B3LYP level for their molecular characteristics, such as dipole moment, electronic energy, HOMO, LUMO, energy gap, global quantum reactivity descriptors, and MEP scale and structure and compared to the reference compound acarbose (Table S2 in ESI file†). The B3LYP/6-311G level is perfect for medium-sized molecules because it strikes a compromise between precision and computational efficiency. The 6-311G basis set offers enough accuracy for reactivity and stability investigations, whereas B3LYP predicts geometries and electrical properties with reliability. For organic and biomolecular systems, this combination has received extensive validation.[70,71]

3.6.7.1. Dipole moment. It is a measurement of molecule polarity that affects solubility and reactivity.[72] The dipole moment of compound **1** (3.288292), compound **2** (4.502051), compound **8** (2.893935), and compound **9** (3.785607) was substantially lower than that of acarbose (9.201717 debye). But out of all the derivatives, compound **10** had the largest dipole moment (6.387456 debye), suggesting a polarity closest to acarbose. This implies compound **10** might resemble the reference chemical regarding solubility and intermolecular interactions.

3.6.7.2. Frontier molecular orbitals (HOMO–LUMO) analysis. In quantum chemistry, the Frontier Molecular Orbitals (FMOs), which are the Highest Occupied Molecular Orbital (HOMO) and Lowest Unoccupied Molecular Orbital (LUMO), along with their energy gap, are highly helpful characteristics. One way to interpret HOMO is as the outermost orbital with electrons, signifying the ability to give an electron, and LUMO as the innermost orbital with free spaces, signifying the ability to accept an electron. Both intramolecular charge transfer (ICT) within the molecule and reduced chemical reactivity, which suggests stronger kinetic stability, are indicated by a lower HOMO–LUMO energy gap value.[73]

Acarbose has an energy gap of 0.23029 eV since its HOMO energy is −0.21573 eV and its LUMO energy is −0.01456 eV. Its strong stability and mild reactivity are reflected in this comparatively large energy gap, which is in line with its biological function as an enzyme inhibitor. However, there are significant differences in the FMO energies of the compounds.

The HOMO values of molecules compounds **1**, **2**, **8**, **9**, and **10** ranged from −0.23222 eV (compound **1**) to −0.19685 eV (compound **8**), suggesting that their electron-donating potential differed little from that of acarbose. All of the derivatives had negative LUMO values, but compound **10** had the lowest −0.07028 eV, indicating a higher capacity to receive electrons than acarbose. In comparison to acarbose, compound **1** has the smallest energy gap (0.31547 eV), suggesting more chemical reactivity and decreased stability.

As compounds **8** and **10** were the lead compounds in *in vitro* and *in vivo* studies so they both have better electron-donating and accepting capacities than acarbose, as seen by their lower HOMO values (−0.22072 eV and −0.19694 eV, respectively) and

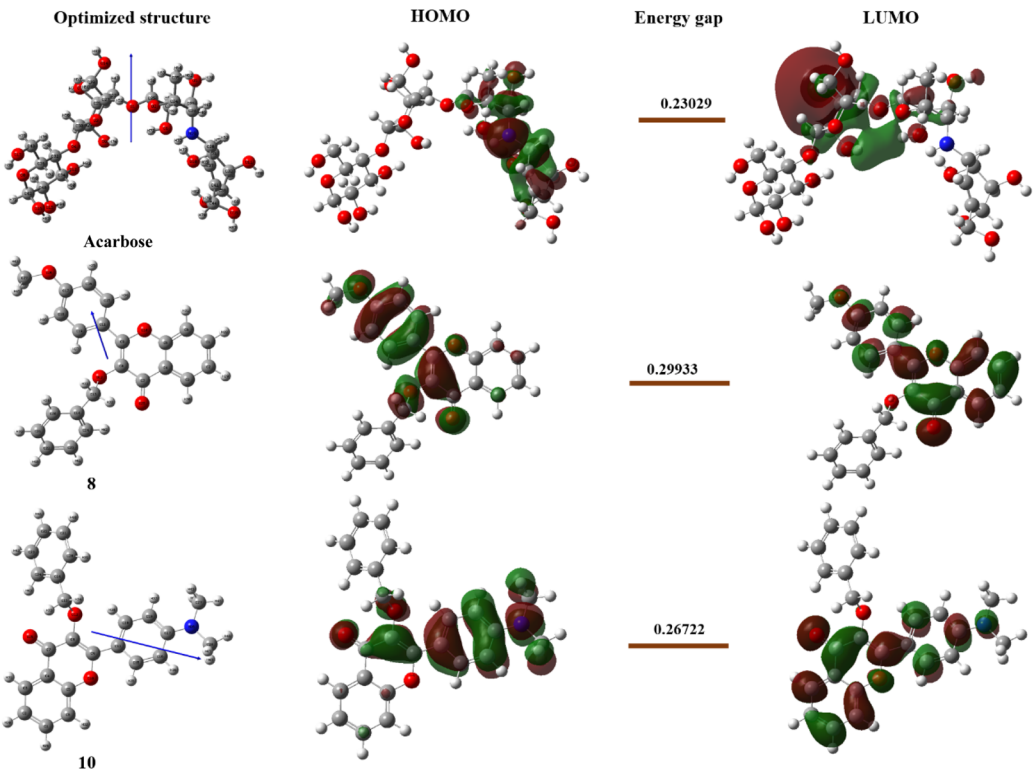

Fig. 5 Optimized structure and HOMO–LUMO diagram of acarbose in comparison with **8** and **10**.

negative LUMO energies (−0.07861 eV and −0.07028 eV, respectively) as shown in Fig. 5.

With compound **8** at 0.29933 eV and compound **10** at 0.26722 eV, the derivatives' energy gaps are also noticeably smaller, suggesting more chemical reactivity and less stability. Because of their decreased stability, these compounds might be more suited for particular uses that call for higher reactivity, including enzyme inhibition or redox reactions. The variations in HOMO–LUMO energies and energy gaps between acarbose and its derivatives demonstrate how structural changes affect their electrical characteristics and point to possible improvements in their functional performance as a result of increased reactivity.[74]

3.6.7.3. Optimized structures. The optimized structures of compounds **1**, **2**, **8**, **9**, **10**, and acarbose were determined using DFT analysis at the basic set of 6-311G/B3LYP (Fig. 5). The distribution of electrons and arrangement of atoms in space are revealed by these optimized geometries, and this information directly affects the compound's chemical and biological behavior.[75] The reference, acarbose, has a complicated, highly branching structure with several functional groups that contain hydroxyl and oxygen. These characteristics help it interact with biological targets like proteins in the body to treat diabetes because of its high polarity and notable dipole moment of 9.201717 debye. Compounds **8** and **10** have altered structures with substitutions that change their electrical characteristics and geometries. For example, the addition of heteroatoms, like nitrogen in compound **10**, alters the distribution of electron densities and dipole moments. In comparison to acarbose, these compounds are more reactive due to their enhanced electronic delocalization caused by the higher conjugation.

3.6.7.4. Electron affinity (A) and ionization potential (I). The electron affinity (A) shows the energy shift that occurs when an electron is introduced, whereas the ionization potential (I) shows the energy needed to remove an electron. Acarbose has an electron affinity of 0.01456 eV and an ionization potential of 0.21573 eV.

Compound **1** has the highest ionization potential (0.23222 eV) of all the derivatives, indicating that it is more resilient to electron removal than acarbose. The strongest electron affinities are shown by compound **1** (0.08325 eV) and compound **9** (0.08672 eV), suggesting that they may be electron acceptors.

3.6.7.5. Global reactivity descriptors. The chemical reactivity and stability of the molecules are shown by the global reactivity descriptors, which include chemical potential (μ), electronegativity (χ), chemical hardness (η), and softness (S):

Chemical potential (μ): the chemical potential (μ) of compound **1** is the greatest at 0.157735 eV, suggesting that it is more stable than acarbose (0.115145 eV).

Electronegativity (χ): in comparison to compound **1** (−0.157735 eV) and the other derivatives, acarbose has a lower electronegativity (−0.115145 eV), indicating a diminished propensity to attract electrons.

Chemical hardness (η): acarbose is comparatively softer (0.100585 eV), suggesting lesser stability and more reactivity, while compound **1** is the hardest chemical (0.074485 eV), followed by compound **10** (0.063405 eV).

Chemical softness (S): in comparison to the derivatives, where compound **2** (16.8535 eV) and compound **10** (15.7903 eV) are less reactive, acarbose has the highest softness value (9.941840 eV), indicating that it is more reactive.

3.6.7.6. Electrophilicity and nucleophilicity indices. Acarbose (0.263625 eV) has a lower electrophilicity index (ω) than its derivatives, compound **1** (0.66806 eV) and compound **9** (0.7091 eV), which indicate a stronger propensity to take electrons. Acarbose (7.165634) has a higher nucleophilicity index (N) than its derivatives, suggesting a stronger capacity for electron donation.

3.6.7.7. MEP scale and structure. A visual tool for comprehending positive, negative, and neutral electrostatic potential regions in relation to color grading and a molecule's relative polarity is the molecular electrostatic potential (MEP). These surfaces also show the charge density, molecular size, molecular structure, and chemically reactive sites of molecules. The various hues on the molecule's MESP surface correspond to different electrostatic potential regions, such as light blue, slightly electron deficient, yellow, slightly electron-rich, green neutral, and red, electron-rich, partially negative charge. The electron density distribution and reactivity patterns for acarbose (reference), compounds **8**, and **10** are depicted in the molecular electrostatic potential (MEP) maps.[76]

The MEP map for acarbose shows areas of electrophilic activity (blue) and very electron-rich areas (red) near oxygen-containing functional groups, which may indicate potential sites for nucleophilic interactions.[77] Compound **8** shows an even distribution with slightly fewer electron density peaks due to modifications in the molecular structure which restrict reactivity. However, compound **10** shows localized electron-rich regions near oxygen atoms and electron-deficient regions surrounding specific structural features, suggesting the possibility of selective interaction. The MEP scale illustrates the gradual transition from electron-rich (red) to electron-deficient (blue), which aids in understanding molecular polarity and chemical reactivity.

Acarbose has the maximum electron density around hydroxyl groups, compound **8** has a more balanced electrical profile, and compound **10** has a more polarized distribution as shown in Fig. 6. Overall, these compounds' MEP structures show their reactive regions. These differences are essential for comprehending their biological activity, ability to inhibit enzymes, and general molecular behavior in certain applications.[78]

In contrast to acarbose, the derivatives exhibit distinct electrical and molecular properties that influence their stability and reactivity. Compound **10** has a moderate chemical potential and a strong dipole moment, making it most similar to acarbose in terms of polarity. While compound **1**, which has the smallest energy gap, has the most chemical reactivity, compound **2**, with its high hardness and ionization potential, has the best stability. The compounds may be used in specific applications, according to our conclusions about their stability and reactivity profiles.

3.6.8. Drug-likeness studies. The analysis highlights a spectrum of molecular properties across the ten compounds

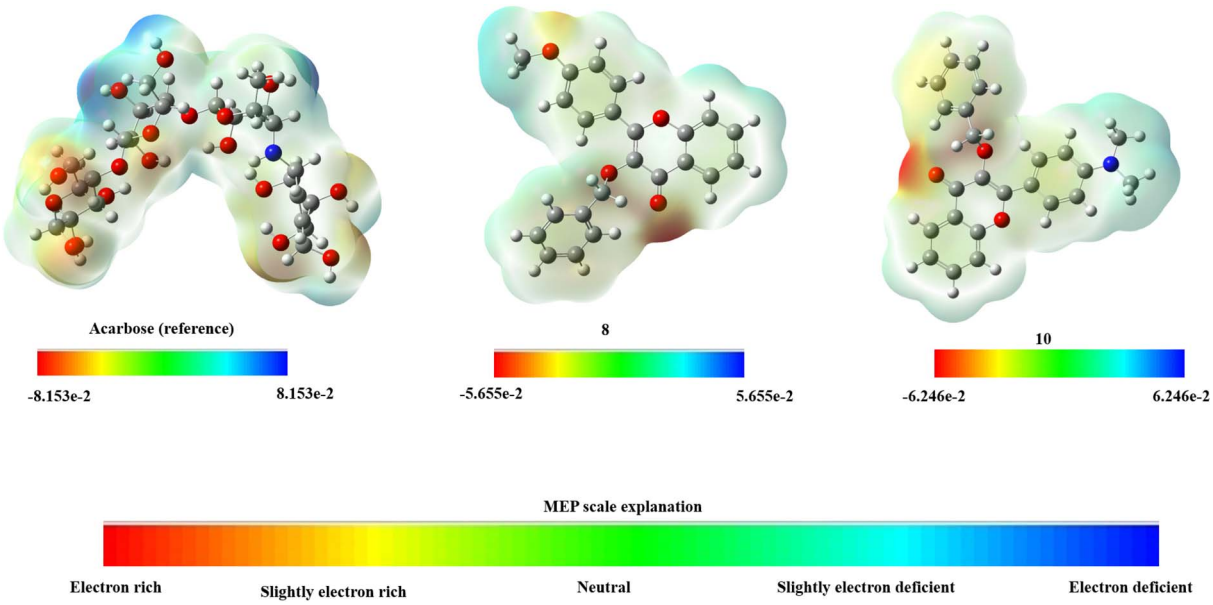

Fig. 6 MEP structure and scale of acarbose, **8** and **10** and also the MEP scale illustration.

Table 7 Drug–likeness properties of target compounds (**1–10**)[a]

Compound no.	Mol. formula	Mol. wt (g mol^{-1})	No. HBA[a]	No. HBD[b]	*M* log *P*[c]	Mol. log *S*[d] (mg L^{-1})	Mol. vol A^3	Drug-likeness model score	Violation	Lipinski's RO5
1	$C_{22}H_{16}O_3$	328.11	3	0	3.08	1.68	333.12	0.00	0	Yes
2	$C_{34}H_{25}NO_3$	495.18	3	0	5.00	0.33	497.20	−0.07	1	Yes
3	$C_{23}H_{18}O_3$	342.13	3	0	3.29	1.01	354.06	0.22	0	Yes
4	$C_{20}H_{14}O_3S$	334.07	4	0	2.67	2.35	326.88	−0.05	0	Yes
5	$C_{22}H_{15}ClO_3$	362.07	3	0	3.56	0.37	350.32	0.58	0	Yes
6	$C_{22}H_{15}NO_5$	373.36	5	0	2.07	1.87	358.19	−0.35	0	Yes
7	$C_{22}H_{15}NO_5$	373.36	5	0	2.07	2.08	358.11	−0.23	0	Yes
8	$C_{23}H_{18}O_4$	358.12	4	0	2.71	2.25	364.97	0.44	0	Yes
9	$C_{20}H_{14}O_4$	318.32	4	0	1.82	8.46	318.56	−0.11	0	Yes
10	$C_{24}H_{21}NO_3$	371.43	3	0	2.92	2.70	382.68	0.13	0	Yes

[a] The table above depicts all Lipinski's RO5 components, *i.e.* [a]number of hydrogen-bond acceptors. [b]Number of hydrogen-bond donors. [c]Octanol–water partition coefficient. [d]Measured solubility.

(Table 7), with compounds **1**, **3**, **4**, **8**, and **10** demonstrating balanced profiles of lipophilicity, solubility, and compliance with drug-likeness criteria. Compounds **5**, **6**, **7**, and **9**, while structurally similar, exhibited slightly lower drug-likeness scores but retained favorable characteristics. In contrast, compound **2**'s high molecular weight and low solubility suggest challenges in drug development despite its potent lipophilicity. Henceforth, the data suggest that several of these compounds warrant further investigation for their potential therapeutic applications, particularly those complying with Lipinski's rule and exhibiting favorable pharmacokinetic properties.

4. Conclusions

This study successfully identified 3-benzyloxyflavone derivatives (**1–10**) as potent β-glucosidase inhibitors through a multidisciplinary approach encompassing experimental and computational evaluations. The *in vitro* and *in vivo* assessments demonstrated that all synthesized compounds (**1–10**) exhibited remarkable inhibitory activity against β-glucosidase, with IC_{50} values ranging from 0.17 μM to 1.02 μM. This performance significantly surpassed the reference standard, acarbose (IC_{50} = 34.09 μM). Among the tested derivatives, compounds **3** (IC_{50} = 0.28 μM), **8** (IC_{50} = 0.17 μM), and **10** (IC_{50} = 0.25 μM) exhibited the highest potency. Acute toxicity evaluations confirmed that the compounds were well-tolerated at doses up to 100 mg kg^{-1}. Subsequent *in vivo* investigations focused on the anti-hyperglycemic potential of six selected compounds (**3**, **5**, **6**, **7**, **8**, and **10**), chosen based on their superior β-glucosidase inhibitory activity. The antidiabetic efficacy of these compounds **3**, **5**, **6**, **7**, **8**, and **10** was further validated using a PGLT-induced diabetic rat model, where they demonstrated a spectrum of good to excellent antihyperglycemic effects. Kinetic analysis indicated that compounds **8** and **10** acted as competitive inhibitors of β-glucosidase. The SAR study revealed that the

nature and position of electron-donating substituents were critical for enhancing inhibitory potency. Molecular docking studies of compounds **8** and **10**, complemented by MD simulations for compound **8**, demonstrated robust and stable interactions with the enzyme's active site, corroborating their molecular binding capabilities. DFT calculations for key compounds (**1**, **2**, **8**, **9**, and **10**) provided deeper insights into their electronic properties and reactivity, further validating their potential as inhibitors. Drug-likeness assessments indicated favorable pharmacokinetic profiles for all synthesized derivatives (**1–10**), supporting their viability as drug candidates. This comprehensive investigation provides a strong foundation for the design and optimization of β-glucosidase inhibitors, offering valuable insights for the development of novel antidiabetic agents. Future studies will focus on advancing the most promising compounds toward preclinical and clinical evaluations.

Ethical statement

The treatment of the animals adhered to the guidelines outlined in the "Animal Bylaws 2008 of the University of Malakand (Scientific Procedures Issue I)." Ethical approval for the study was obtained from the Ethical Committee of the Department of Pharmacy, in accordance with the Animal Bylaws 2008 of the University of Malakand, as per notification no. Pharm/EC-Thzp/41-08/21.

Data availability

All the data is provided in the manuscript and ESI files.†

Author contributions

Nafeesa Naeem: experimental work performance, data analysis, and collection, performed enzyme inhibition activity, software, first-draft preparation; Ehsan Ullah Mughal: supervision, main idea, methodology, resources, reviewing and editing, final writing the manuscript.

Conflicts of interest

Authors have no conflict of interest to declare.

Acknowledgements

The authors acknowledge the Department of Chemistry, University of Gujrat, for providing the necessary laboratory facilities for the successful completion of this research.

References

1 E. Karakılıç, S. Durmuş, S. Sevmezler, O. Şahin and A. Baran, *Bioorg. Med. Chem.*, 2018, **26**, 4276–4287.
2 Y. Bhatia, S. Mishra and V. Bisaria, *Crit. Rev. Biotechnol.*, 2002, **22**, 375–407.
3 J. R. K. Cairns and A. Esen, *Cell. Mol. Life Sci.*, 2010, **67**, 3389.
4 E. Beutler, *Science*, 1992, **256**, 794–799.
5 Y. Gao, J. Duan, X. Dang, Y. Yuan, Y. Wang, X. He, R. Bai, X.-Y. Ye and T. Xie, *J. Enzyme Inhib. Med. Chem.*, 2023, **38**, 2195991.
6 R. R. Singhania, A. K. Patel, R. K. Sukumaran, C. Larroche and A. Pandey, *Bioresour. Technol.*, 2013, **127**, 500–507.
7 A. V. Morant, K. Jørgensen, C. Jørgensen, S. M. Paquette, R. Sánchez-Pérez, B. L. Møller and S. Bak, *Phytochemistry*, 2008, **69**, 1795–1813.
8 M. Bhat, *Biotechnol. Adv.*, 2000, **18**, 355–383.
9 Y. Chen, Y. Deng, Y. Li, Y. Qin, Z. Zhou, H. Yang and Y. Sun, *ACS Appl. Mater. Interfaces*, 2024, **16**, 21546–21556.
10 R. Li, P. Luo, Y. Guo, Y. He and C. Wang, *Expert Opin. Drug Saf.*, 2024, 1–5.
11 J. Zhu, X. Jiang, X. Luo, R. Zhao, J. Li, H. Cai, X. Y. Ye, R. Bai and T. Xie, *Drug Dev. Res.*, 2023, **84**, 718–735.
12 R. Kumar, S. Singh and O. V. Singh, *J. Ind. Microbiol. Biotechnol.*, 2008, **35**, 377–391.
13 A. Esen, Glucosidases: Overview, in *ACS Symposium Series*, American Chemical Society, 1993, vol. 533, p. 1.
14 Q. Q. Lu, Y. M. Chen, H. R. Liu, J. Y. Yan, P. W. Cui, Q. F. Zhang, X. H. Gao, X. Feng and Y. Z. Liu, *Drug Dev. Res.*, 2020, **81**, 1037–1047.
15 E. U. Mughal, J. Ashraf, E. M. Hussein, Y. Nazir, A. S. Alwuthaynani, N. Naeem, A. Sadiq, R. I. Alsantali and S. A. Ahmed, *ACS Omega*, 2022, **7**, 17444–17461.
16 A. T. Rufino, V. M. Costa, F. Carvalho and E. Fernandes, *Med. Res. Rev.*, 2021, **41**, 556–585.
17 R. J. Obaid, E. U. Mughal, N. Naeem, A. Sadiq, R. I. Alsantali, R. S. Jassas, Z. Moussa and S. A. Ahmed, *RSC Adv.*, 2021, **11**, 22159–22198.
18 K. Wen, X. Fang, J. Yang, Y. Yao, K. S. Nandakumar, M. L. Salem and K. Cheng, *Curr. Med. Chem.*, 2021, **28**, 1042–1066.
19 A. Ullah, S. Munir, S. L. Badshah, N. Khan, L. Ghani, B. G. Poulson, A.-H. Emwas and M. Jaremko, *Molecules*, 2020, **25**, 5243.
20 S. J. Maleki, J. F. Crespo and B. Cabanillas, *Food Chem.*, 2019, **299**, 125124.
21 I. Górniak, R. Bartoszewski and J. Króliczewski, *Phytochem. Rev.*, 2019, **18**, 241–272.
22 L. Ciumărnean, M. V. Milaciu, O. Runcan, Ş. C. Vesa, A. L. Răchişan, V. Negrean, M.-G. Perné, V. I. Donca, T.-G. Alexescu and I. Para, *Molecules*, 2020, **25**, 4320.
23 E. U. Mughal, A. Sadiq, M. Ayub, N. Naeem, A. Javid, S. H. Sumrra, M. N. Zafar, B. A. Khan, F. P. Malik and I. Ahmed, *J. Biomol. Struct. Dyn.*, 2021, **39**, 6154–6167.
24 J. Ashraf, E. U. Mughal, A. Sadiq, M. Bibi, N. Naeem, A. Ali, A. Massadaq, N. Fatima, A. Javid and M. N. Zafar, *J. Biomol. Struct. Dyn.*, 2021, **39**, 7107–7122.
25 L. Chen, H. Teng, Z. Xie, H. Cao, W. S. Cheang, K. Skalicka-Woniak, M. I. Georgiev and J. Xiao, *Crit. Rev. Food Sci. Nutr.*, 2018, **58**, 513–527.
26 P. Kachlicki, A. Piasecka, M. Stobiecki and Ł. Marczak, *Molecules*, 2016, **21**, 1494.
27 L. Chen, Z. Jiang, L. Yang, Y. Fang, S. Lu, O. U. Akakuru, S. Huang, J. Li, S. Ma and A. Wu, *Chin. J. Chem.*, 2023, **41**, 199–206.

28 L. Chepeleva, D. Tarasenko, A. Chumak, O. Demidov, A. Snizhko, O. Kolomoitsev, V. Kotliar, E. Gladkov, A. Tatarets and A. Kyrychenko, *Funct. Mater.*, 2023, **30**, 495.
29 V. Gopal, J. Sudhakaran, N. Ramachandran, T. K. Mana, A. R. Kana, A. O. Nair, P. Mohan, T. Madhusudhan, S. Shanmugaraju and P. Nanjan, *Sens. Diagn.*, 2024, **3**, 1263–1271.
30 S. Tang, B. Wang, X. Liu, W. Xi, Y. Yue, X. Tan, J. Bai and L. Huang, *Food Front.*, 2025, 218–247.
31 L. Kang, X.-H. Gao, H.-R. Liu, X. Men, H.-N. Wu, P.-W. Cui, E. Oldfield and J.-Y. Yan, *Mol. Divers.*, 2018, **22**, 893–906.
32 R. Nath, S. Manna, S. Panda, A. Maity, K. Bandyopadhyay, A. Das, S. A. A. Khan, B. Debnath and M. J. Akhtar, *Chem. Biodiversity*, 2024, e202401899.
33 G. Zeng, Z. Wu, W. Cao, Y. Wang, X. Deng and Y. Zhou, *Nat. Prod. Res.*, 2020, **34**, 1041–1045.
34 M. E. Erkanli, K. El-Halabi and J. R. Kim, *Enzyme Microb. Technol.*, 2023, 110363.
35 Y. Cheng, L. Wang, S. Zhang, W. Jian, B. Zeng, L. Liang and Z. Deng, *Curr. Med. Chem.*, 2024, DOI: **10.2174/0109298673309489240816063313**.
36 A. M. Dirir, M. Daou, A. F. Yousef and L. F. Yousef, *Phytochem. Rev.*, 2022, **21**, 1049–1079.
37 N. Agrawal, M. Sharma, S. Singh and A. Goyal, *Curr. Top. Med. Chem.*, 2022, **22**, 2069–2086.
38 E. B. de Melo, A. da Silveira Gomes and I. Carvalho, *Tetrahedron*, 2006, **62**, 10277–10302.
39 H. Saleem, A. Yaqub, R. Rafique, T. Ali Chohan, D.-e.-S. Malik, M. I. Tousif, U. Khurshid, N. Ahemad, R. Ramasubburayan and K. R. Rengasamy, *Crit. Rev. Food Sci. Nutr.*, 2024, **64**, 9805–9828.
40 J. Zhu, C. Chen, B. Zhang and Q. Huang, *Crit. Rev. Food Sci. Nutr.*, 2020, **60**, 695–708.
41 Y. Cahyana and T. Adiyanti, *Indones. J. Chem.*, 2021, **21**, 512–526.
42 V. Jaitak, *Mini-Rev. Med. Chem.*, 2019, **19**, 762–786.
43 Y. Ji, B. Li, M. Qiao, J. Li, H. Xu, L. Zhang and X. Zhang, *Appl. Microbiol. Biotechnol.*, 2020, **104**, 6587–6600.
44 X. H. Gao, J. J. Tang, H. R. Liu, L. B. Liu and Y. Z. Liu, *Drug Dev. Res.*, 2019, **80**, 438–445.
45 K. Kytidou, M. Artola, H. S. Overkleeft and J. M. Aerts, *Front. Plant Sci.*, 2020, **11**, 357.
46 F. Sok Yen, C. Shu Qin, S. Tan Shi Xuan, P. Jia Ying, H. Yi Le, T. Darmarajan, B. Gunasekaran and S. Salvamani, *Evidence-Based Complementary Altern. Med.*, 2021, **2021**, 2057333.
47 J. Ashraf, E. U. Mughal, A. Sadiq, N. Naeem, S. A. Muhammad, T. Qousain, M. N. Zafar, B. A. Khan and M. Anees, *J. Mol. Struct.*, 2020, **1218**, 128458.
48 R. Mehmood, E. U. Mughal, E. B. Elkaeed, R. J. Obaid, Y. Nazir, H. A. Al-Ghulikah, N. Naeem, M. M. Al-Rooqi, S. A. Ahmed and S. W. A. Shah, *ACS Omega*, 2022, **7**, 30215–30232.
49 H. A. Al-ghulikah, E. U. Mughal, E. B. Elkaeed, N. Naeem, Y. Nazir, A. Y. A. Alzahrani, A. Sadiq and S. W. A. Shah, *J. Mol. Struct.*, 2023, **1275**, 134658.
50 M. Alamzeb, S. W. A. Shah, H. Hussain, M. Zahoor, S. Ahmad, E. U. Mughal, S. Ahmad, I. Ullah, S. Khan and A. Ullah, *ACS Omega*, 2024, **9**, 9813–9822.
51 R. Mehmood, A. Sadiq, R. I. Alsantali, E. U. Mughal, M. A. Alsharif, N. Naeem, A. Javid, M. M. Al-Rooqi, G.-e.-S. Chaudhry and S. A. Ahmed, *ACS Omega*, 2022, **7**, 3775–3795.
52 V. R. Shah, J. D. Bhaliya and G. M. Patel, *J. Basic Clin. Physiol. Pharmacol.*, 2021, **32**, 197–214.
53 S. Bouchagra, F. Benamia and Z. Djeghaba, *Res. J. Pharm., Biol. Chem. Sci.*, 2016, **7**, 2493–2505.
54 C. E. Cassidy and W. N. Setzer, *J. Mol. Model.*, 2010, **16**, 311–326.
55 W. Jorgensen and J. Chandrasekhar, *J. Chem. Phys.*, 1983, **79**, 926.
56 K. A. Qureshi, I. Al Nasr, W. S. Koko, T. A. Khan, M. Q. Fatmi, M. Imtiaz, R. A. Khan, H. A. Mohammed, M. Jaremko and A.-H. Emwas, *Antibiotics*, 2021, **10**, 887.
57 B. Hess, H. Bekker, H. J. Berendsen and J. G. Fraaije, *J. Comput. Chem.*, 1997, **18**, 1463–1472.
58 H. Grubmüller, H. Heller, A. Windemuth and K. Schulten, *Mol. Simul.*, 1991, **6**, 121–142.
59 U. Essmann, L. Perera, M. L. Berkowitz, T. Darden, H. Lee and L. G. Pedersen, *J. Chem. Phys.*, 1995, **103**, 8577–8593.
60 B. J. Grant, L. Skjærven and X. Q. Yao, *Protein Sci.*, 2021, **30**, 20–30.
61 J. Huang and A. D. MacKerell Jr, *J. Comput. Chem.*, 2013, **34**, 2135–2145.
62 R. Srivastava, F. A. Al-Omary, A. A. El-Emam, S. K. Pathak, M. Karabacak, V. Narayan, S. Chand, O. Prasad and L. Sinha, *J. Mol. Struct.*, 2017, **1137**, 725–741.
63 W. Shoukat, M. Hussain, A. Ali, N. Shafiq, A. H. Chughtai, B. Shakoor, A. Moveed, M. N. Shoukat, M. Milošević and M. Mohany, *J. Mol. Struct.*, 2025, **1320**, 139614.
64 K. Yamamoto, H. Miyake, M. Kusunoki and S. Osaki, *FEBS J.*, 2010, **277**, 4205–4214.
65 Y. Xu, Y. Wang, K. Liu, Y. Peng, D. Yao, H. Tao, H. Liu and G. Song, *IUCrJ*, 2019, **6**, 996–1006.
66 K. Lisina and S. Piramanayagam, *World. J. Pharm. Sci.*, 2014, 283–293.
67 M. E. Gondokesumo and I. M. Kurniawan, *J. Basic Clin. Physiol. Pharmacol.*, 2019, **30**, 20190282.
68 N. Shafiq, B. Shakoor, N. Yaqoob, S. Parveen, S. Brogi, A. Mohammad Salamatullah, M. Rashid and M. Bourhia, *J. Biomol. Struct. Dyn.*, 2024, 1–22.
69 F. Sezer Senol, M. Tareq Hassan Khan, G. Orhan, E. Gurkas, I. Erdogan Orhan, N. Subutay Oztekin and F. Ak, *Curr. Top. Med. Chem.*, 2014, **14**, 1469–1472.
70 W. J. Hehre, R. Ditchfield and J. A. Pople, *J. Chem. Phys.*, 1972, **56**, 2257–2261.
71 C. Lee, W. Yang and R. G. Parr, *Phys. Rev. B:Condens. Matter Mater. Phys.*, 1988, **37**, 785.
72 S. Böhm and O. Exner, *Phys. Chem. Chem. Phys.*, 2004, **6**, 510–514.
73 V. Choudhary, A. Bhatt, D. Dash and N. Sharma, *J. Comput. Chem.*, 2019, **40**, 2354–2363.

74 J. Singh, M. S. Khan and S. Uddin, *Polym. Bull.*, 2023, **80**, 3055–3083.
75 L. Fan and T. Ziegler, *J. Chem. Phys.*, 1991, **95**, 7401–7408.
76 P. Govindasamy and S. Gunasekaran, *Spectrochim. Acta, Part A*, 2015, **136**, 1543–1556.
77 Ö. Mıhçıokur and T. Özpozan, *J. Mol. Struct.*, 2017, **1149**, 27–41.
78 E. S. Marinho and M. M. Marinho, *Int. J. Sci. Eng. Res.*, 2016, **7**, 1264.